TAB connection for the Silicon Strip Detector in STAR

STAR NOTE 0431

C. Suire, L. Arnold, J. Baudot, D. Bonnet, J.P. Coffin, M. Germain, C. Gojak, M. Guedon, B. Hippolyte, C. Kuhn, J.R. Lutz, A. Tarchini.

Institut de Recherches Subatomiques-IReS - IN2P3/CNRS - ULP
BP28, F 67037 Strasbourg Cedex 02 - France

A. Boucham, N. Bouillo, S. Bouvier, J. Castillo, D. Charrier, L. Conin, C. Drancourt, B. Erazmus, L. Gaudichet, G. Guilloux, L. Lakahal-Ayat, F. Lefevre, L. Martin, T. Milletto, C. Le Moal, O. Ravel, C. Renard, L.M. Rigalleau, C. Roy, D. Roy.

Laboratoire SUBATECH, Université de Nantes - Ecoles des Mines de Nantes -IN2P3/CNRS
La Chantrerie, F 44070 Cedex 03 - France

Abstract

The inner part of the STAR detector [1] is composed of the vertex tracker, three layers of Silicon Drift Detector (SVT) and one layer of Silicon Strip Detector (SSD). The Silicon Strip Detector layer is a cylinder of 320 double-sided detectors with 768 strips per side. In order to connect the large number of microstrips (~ 500000) of the SSD barrel to the Front End Electronics, a connection process (Tape Automated Bonding) has been chosen to replace the classical wire-bonding technique. The prototypes of modules have been successfully completed and tested in- and off-beam. This report summarizes the tests performed and gives the conclusions about the TAB reliability and efficiency.

[1] http://www.star.bnl.gov/STAR/

1 Introduction

In the STAR experiment installed at the RHIC collider, the internal tracker is made of 4 layers of silicon detectors. The three inner layers (Silicon Vertex Tracker) use silicon drift detectors ([1], [2], which has just been installed and succesfully tested), the outermost uses one silicon strip detectors ([3], to be installed in 2002). According to simulations described in [3],[4], the SSD layer is an important upgrade in terms of short-lived particle reconstruction and more generally, particle tracking efficiency due to its ability to improve the matching between TPC tracks and SVT hits.

The SSD sub-detector is a cylinder of 20 carbon ladders surrounding the SVT, at a radius of 23 cm. Each carbon ladder supports 16 silicon strip detectors which provide a two dimensional position of particles (rΦ,Z) and energy loss information. The 320 silicon strip detectors are double-sided with 768 strips on each side, i.e $\sim$ 500,000 analog channels for the whole SSD barrel. A single detection module is made of one silicon strip detector connected to its Front End Electronics. For each side of the detector, an hybrid supports the 6 readout chips. Furthermore, in order to produce a detection module as compact and reliable as possible, the two hybrids have to be folded over the detector, thus implying a flexibility of the detector-hybrid connection.

Facing those two problems: a huge number of electrical connections to perform and the ability to fold the FEE over the detector, we have investigated a new technique, Tape Automated Bonding (TAB) [6], [7] described in the next section [2]. In the third section is explained the principle of the tests made to evaluate the performances of this kind of connection. Results are given in the sections fourth and fifth .

[2]this process has been used for years in microelectronics industry but not in high energy physics experiments. For the time being, the only other experiment which will use this technique is ALICE (CERN) for the TPC [10] and the silicon strip detectors layers

2 TAB (Tape Automated Bonding) connection

2.1 Description

The classical way to interconnect silicon strip detectors to their readout electronics is wire-bonding. In this method, an aluminium wire ($\sim$ 10 μm radius) is welded by ultrasound between the two pieces to be connected. TAB is based on a different principle. First of all, a mask is created which display each interconnecting strip between components. This mask is then used to etch these copper strips onto a kapton tape. To achieve the connection, the tape is superimposed on top of the components (pad to pad matching), then ultrasound applied on each pad, simultaneously with heating, to insure the welding.
Consequently in this technique, there is no independent bond but rather a flexible ensemble of cables which holds all the copper micro-strips, thus providing a better mechanical resistance which allows to bend all the interconnections at once. The first two figures show photographs of the tape used to connect the front-end electronics to the silicon strip detector and to the hybrid (Fig.1). Fig.2 shows the same tape after connection to the ALICE128C readout chip [5]. It should be emphasize that only one design of tape is used to connect the 12 readout chips to the silicon strip detector.

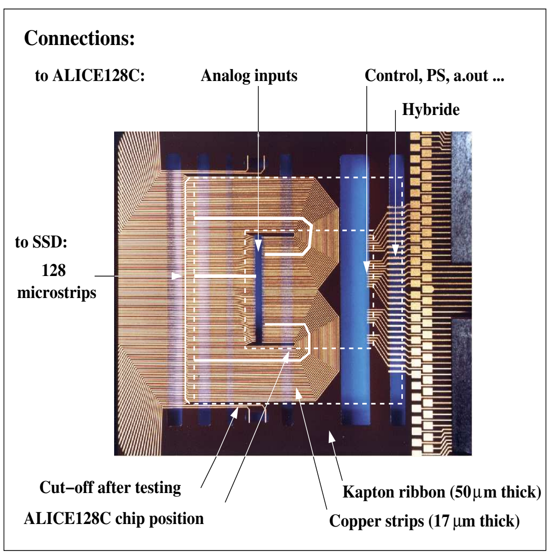

Figure 1: TAB tape : copper strips are visible. They provide on the left side 128 connections between μ-strips of a detector and analog inputs of a readout chip and 28 on the right side for the connection to hybrid (controls signals, power supplies, analog-out ...). White lines highlight the three different geometries of copper strips etched on the tape : starting from the bottom, we have 32 bended strips (sort of U shape), then 64 straight strips and finally 32 U shaped strips.

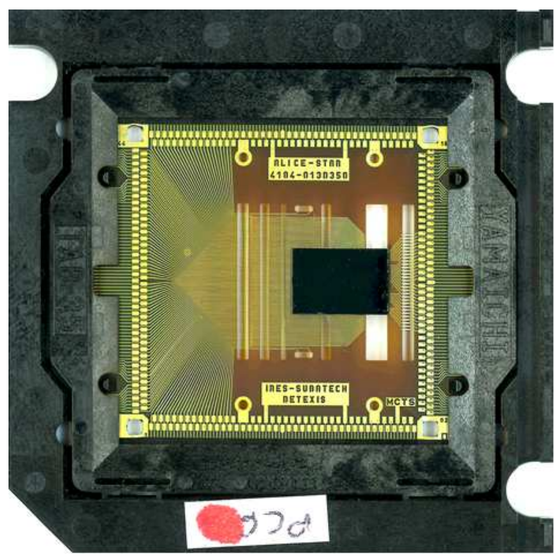

Figure 2: Photograph of an ALICE128C readout chip (black rectangle in the center) connected to TAB tape in its test support, before connection to the other components (strip detector and hybrids). Size of ALICE128C chip is 8640 $\times$ 6080 μm.

2.2 Application

The 320 detection modules that compose the SSD layer are all identical. A module is made of one detector and two hybrids, one dedicated to the readout of the p-side and the other one to the n-side. An hybrid is made of a kapton tape, with printed copper strips, glued on a carbon stiffener. On each hybrid, the FEE (Front End Electronics) includes 6 readout chips ALICE128C, a chip COSTAR (COntrol STAR), specially designed for slow-control (temperature and currents monitoring) [8], and some passive components resistors and capacitors.
Once all the elements are tested and assembled, each hybrid is folded over the detector, so that the two stiffeners are supported by the detector, as shown in Fig.3. The TAB exhibits here its best advantage, allowing, due to its flexibility, to fold hybrids over the detector. A very compact detection module is finally obtained for which total size is almost equal to the active area. This feature makes easier a large angular coverage without overlapping modules.

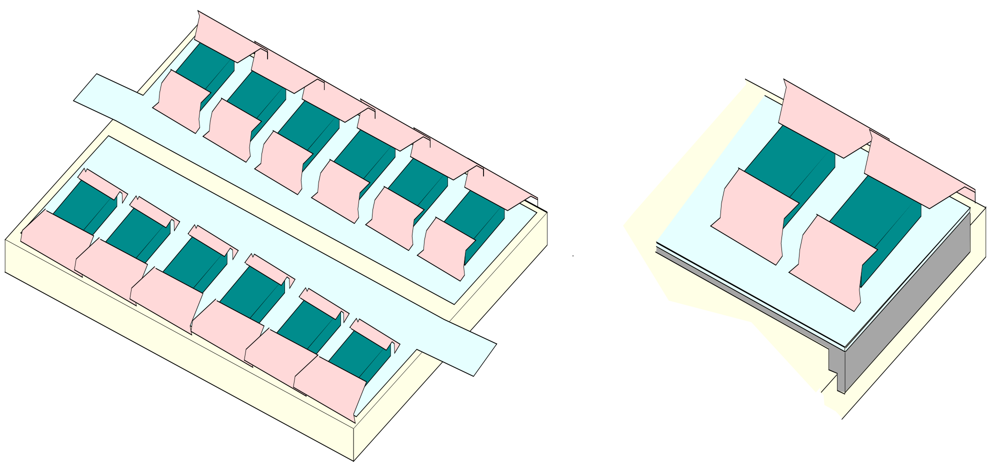

Figure 3: Scheme of an assembled detection module. The first step is the connection of the readout chips (green) on the TAB tape (light red), already shown in Fig.2. Then the analog inputs of the ALICE128C chip are connected to the μ-strips of the the detector (yellow). After that the chips are glued and connected to hybrids (light blue). The COSTAR chip, also located on the hybrid is not represented here. Finally, the hybrids are folded over the detector. On the right part of this figure, a magnified view shows the stiffener (gray) on which the hybrids are glued.

Moreover, due to its design, TAB tape performs the pitch adaptation between the silicon detector microstrips (pitch of 95 μm) and the analog inputs of the readout chip (pitch of 44 μm). This is obtained from the two types of copper strips geometry etched on the tape, as shown in Fig.4.

The total number of electrical connections to achieve is the following :

- connections μstrips-ALICE128C : $2 \times 768 \times 320 = 491520$,
- connections ALICE128C-hybrids : $12 \times 28 \times 320 = 107520$,
- connections COSTAR (wire-bond) : $2 \times 25 \times 320 = 16000$.

The first and the second type are using TAB, making a total number of this kind of connections equal to 598040. A photo of an assembled prototype module, tested in and off-beam is given in Fig.5.

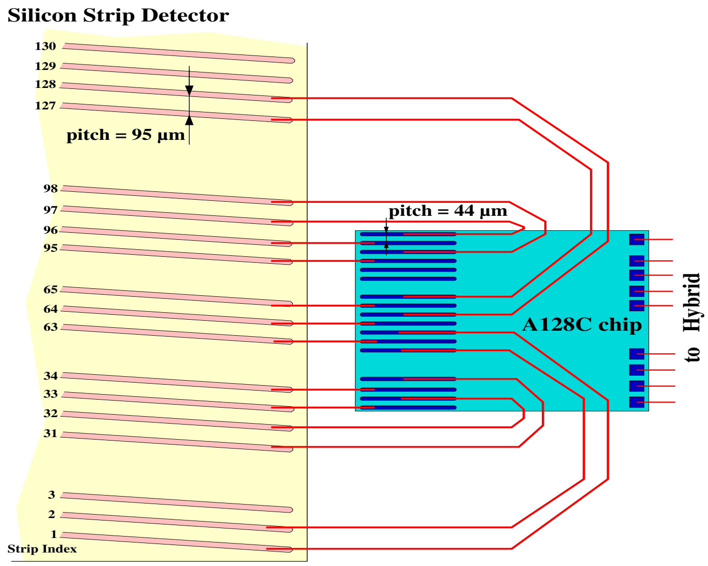

Figure 4: The TAB tape performs the pitch adaptation between silicon microstrips and ALICE128C chip analog inputs.

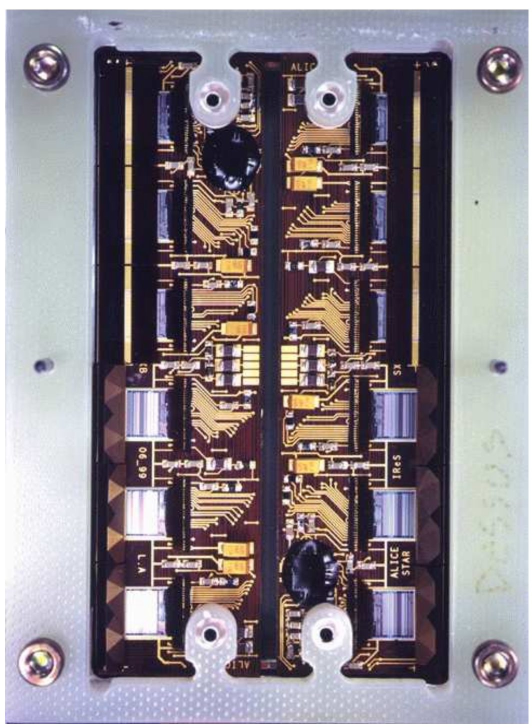

Figure 5: Photo of a STAR detection module (the mechanical frame for easy-handling will be removed before the assembly on ladders). The overall surface (detector + front end readout electronics) is 76×43 mm^2 (the sensitive area is 73×40 mm^2) and less than 10 mm thick.

3 Test procedure and experimental approach

3.1 Test procedure

To consider the different problems which can occur in a detection module construction or/and operation, we may refer to figure 6 where the schematic view of a readout channel is given. When a particle crosses the detector, charges are created, then collected by the strips and driven to the analog inputs of the chip via the TAB. Each channel of the chip ALICE128C amplifies, shapes and stores, as a voltage signal the charges deposited on the corresponding strip. An analog multiplexer allows a sequential readout of the data at 10 MHz rate through an output buffer shared by the 128 channels. Then the multiplexed analog output signal is digitized by ADC and finally written on tape or on disk. This process is run sequentially for the 12 readout chips, and the information of the 1536 detector strips is stored.

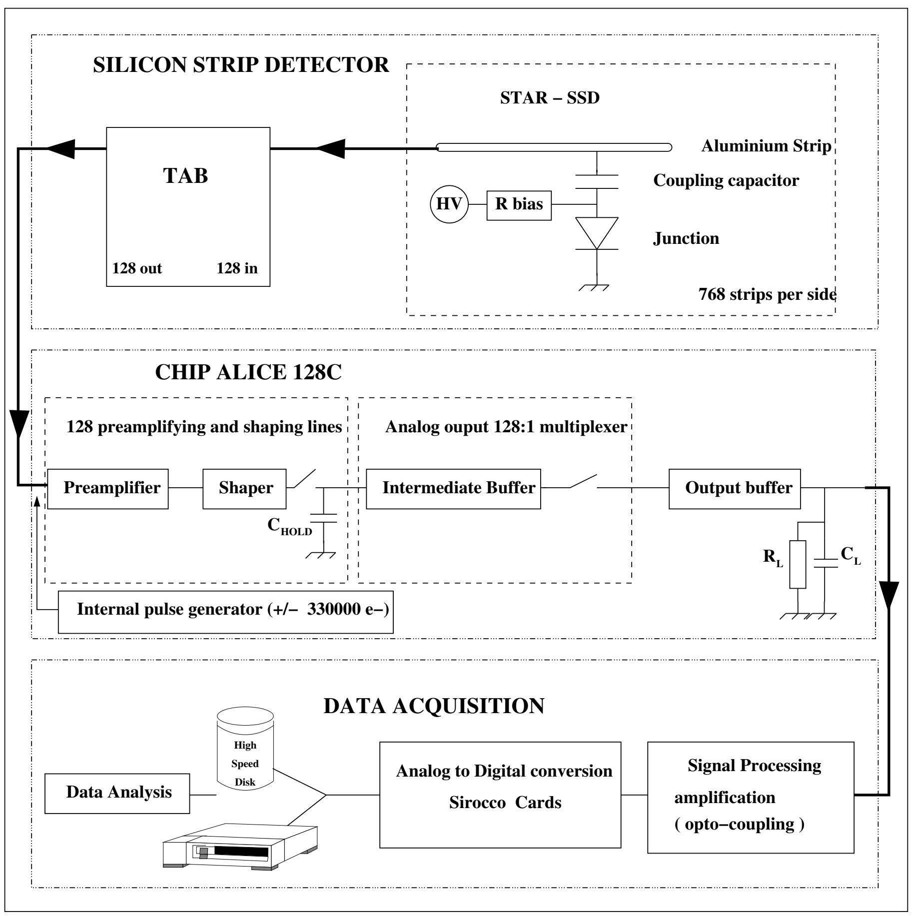

Figure 6: Comprehensive scheme of the readout setup from a detector strip to the analysis of the digitized signal.

The aim of the analysis presented in the following sections is to extract from the data a reliable information about the TAB connection. First, we have to find a variable sensitive to all types of connection problems. Then, a systematic study will allow us to establish the relationship between the behaviour of the variable and the type of defects.

3.2 Data analysis

The raw signal $r_k(n)$, i.e. the value of digitized signal on a detector's strip k for an event n can be expressed as the sum of the following terms : a physical charge $q_k^{phy}(n)$, a random charge $q_k^{rnd}(n)$, the pedestal $p_k(n)$, and the common mode shift $cms(n)$.

$$r_k(n) = q_k^{phy}(n) + q_k^{rnd} + p_k(n) + cms(n) \tag{1}$$

All those quantities have the dimension of a charge measured in ADC counts. The physical signal $q_k^{phy}(n)$ is due to a particle interaction in the detector, the random charge q_k^{rnd} corresponds to the noise. Noise runs have been made for each detection modules, i.e DAQ is triggered by an external pulse generator, removing the term $q_k^{phy}(n)$ in eq.1. Then,

$$r_k(n) = q_k^{rnd} + p_k(n) + cms(n) \tag{2}$$

The common mode shift has a specific value for each chip within an event. In this analysis, we suppose that the cms is negligible in respect of the value of q_k^{rnd}.

Now, we have access to the following variables : the pedestal p_k and its variance $V(r_k)$, which could be interpreted as the convolution of the channel noise with the cms.

$$p_k = \frac{1}{N}\sum_{n=0}^{N} r_k(n) \tag{3}$$

$$V(r_k) = \frac{1}{\sqrt{N-1}}\sqrt{\left|\sum_{n=0}^{N} [r_k(n)]^2 - 1/N\left[\sum_{n=0}^{N} r_k(n)\right]^2\right|} \tag{4}$$

3.3 Defect analysis

We will use the variable $V(r_k)$, calculated for each strip of a detection module, to determine defective channels, and to try to correlate its behavior to the different types of defects.

In Fig.7 is plotted $V(r_k)$ versus the strip index of a detector. We can see that for some channels, the value is clearly higher or lower than the mean : those channels have been tested individually with a β-source (^{90}Sr) and ALICE128C internal test pulse generator [5] to understand the origin of the problem. The internal test pulse generator allows us to deposit, at any of the analog inputs of the ALICE chip, an adjustable current simulating charges created by the passage of charged particle.

In Fig.8 are listed the different cases we have to deal with. On each graph is plotted the pedestal distribution over 900 events, $V(r_k)$ is given by the RMS of the distribution.

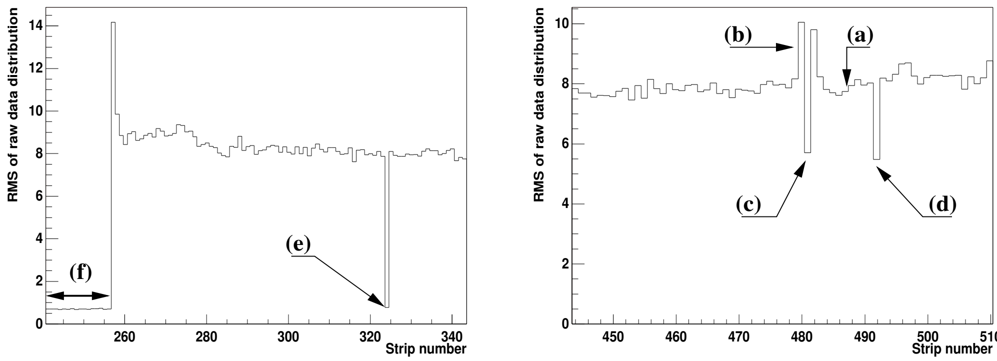

Figure 7: $V(r_k)$ plotted versus the strip index of a p-side detection module.

Case (a), this channel (associated with the strip 487 can be seen also on Fig.7) operates properly : the response to a stimulation of a β-source or to the internal pulse generator, is the expected one. The value of $V(r_k)$ is 7.75 ADC counts.

Case (b), the channel (strip 480) works correctly but the value $V(r_k)$ is higher than the other channels. This is the case of a noisy strip.

Case (c), the channel response (strip 481) is correct with regard to the stimulation with the internal pulse generator, but there is no response to a detector irradiation with the β-source. A possible explanation is an interruption between the aluminium strip of the detector and the analog input of the chip. Detector noise is ignored in the preamplifier and consequently $V(r_k)$ has a lower value. Furthermore, another systematic effect occurs for the case of a not-connected strip : the neighbouring strips $n+1$ and $n-1$ exhibit a $\sim$ 20 % higher $V(r_k)$ value (this is case (b)).

Case (d), the channel (strip 492) does not respond to any stimulation, neither with the β-source nor with the internal pulse generator. The $V(r_k)$ value is comparable to case (c), but the cause is different : in this case, we suppose that the preamplifier for this channel has been destroyed during the TAB process. We do not observe any effects of this defect on neighbouring strips.

Case (e), the channel does not operate (strip 324). The analog output is flat and $V(r_k)$ is very low : preamplifier and shaping blocks in the ALICE chip are certainly broken. Such channels exist on the chip after the production, and are not related to the TAB process.

Case (f), these channels are not read (from strip 129 to 256). The chip has been destroyed during the assembly, and is bypassed during the readout sequence : the information for the 128 corresponding strips is lost. The only noise source is ambient noise, implying a very low value of $V(r_k)$.

The last case that has not been detailed is that of pinholes (leak of current, partial or total, through the coupling capacitor [9]). These defects, intrinsic to silicon strip detector,

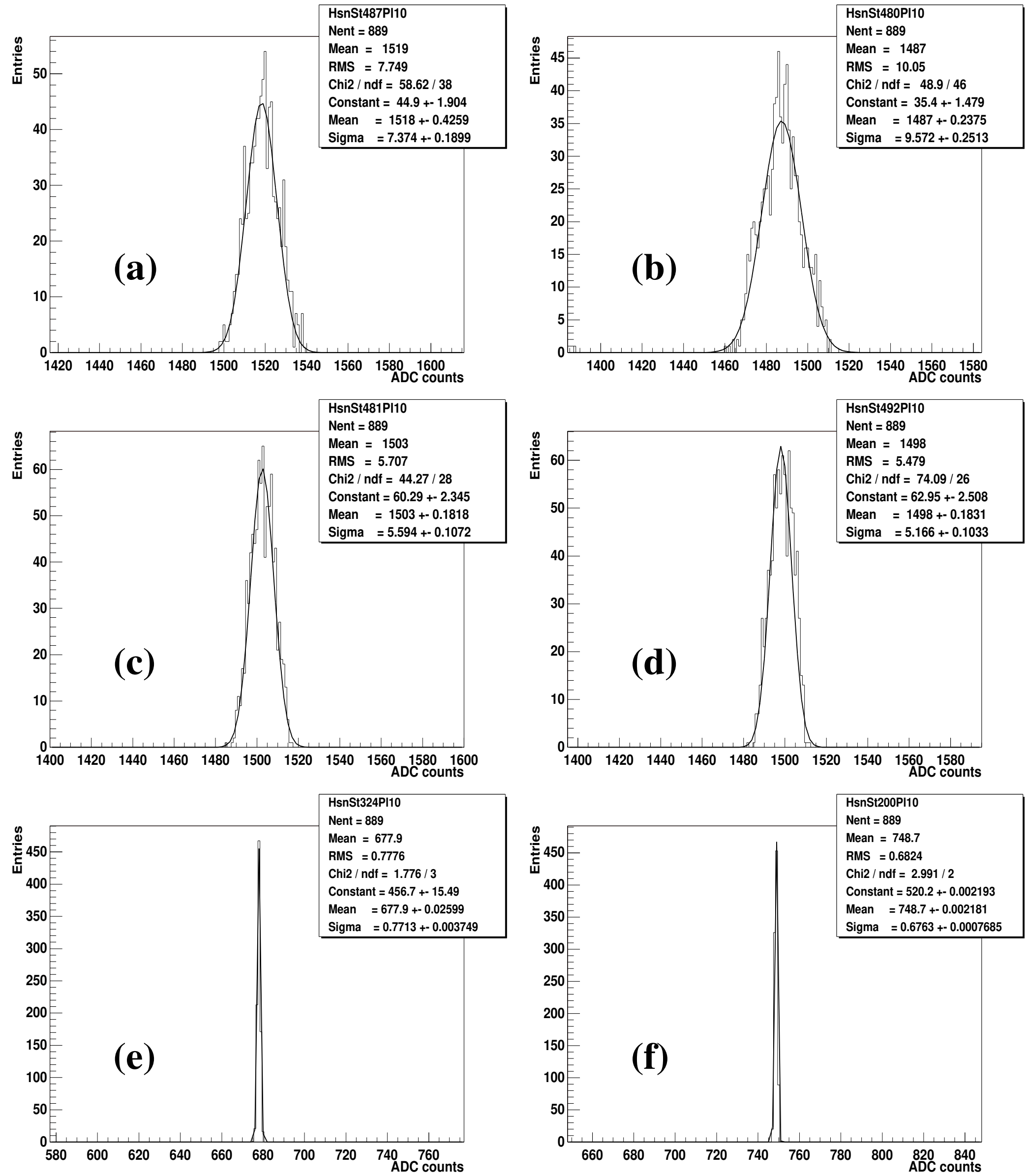

Figure 8: Analog output of channels for the different observed defects. See text for description of the different defects.

are detected by production tests under probe-station. When the detector is connected to electronics, pinholes can also be seen with the method using $V(r_k)$.
The pinholes induce different effects depending on which side they are located on. On the p-side, the channel is sensitive to β-source and internal pulse generator, but the strong distortion of analog output signal makes inefficient the detection of particles. On the n-side, the channel does not respond neither to β-source nor to internal pulse generator, and the neighbouring strips $n+1$ and $n-1$ are noisier : this is comparable to case (c).

More comments about of this behaviour are given in section 5.

4 Results of the analysis of detection module

The four prototype modules studied are at complete final STAR design, and are described in section 1 (see Fig.3, 5), and [3]. The method described in the preceding section is now applied to each detection module, and TAB defects are determined.

4.1 Principle

Before the assembly, all active parts of a detection module are individually tested, allowing for determining where problems do appear in the process and if they are related to the TAB operation. For instance, we present here results of test for the module 1. This module has an important difference, as compared to the three other modules : the hybrids are not folded over the detector.

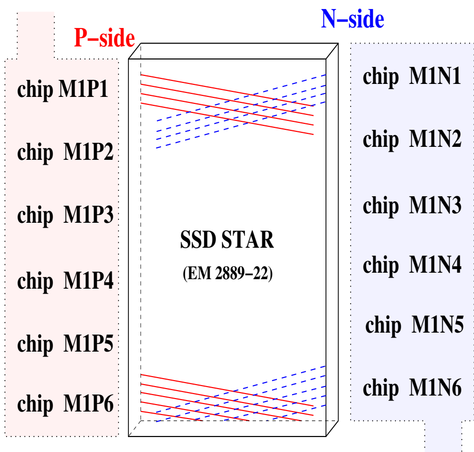

ALICE128C chip on TAB tape (in test frame, Fig.2)		
M1P2	chip broken (before TAB process)	
M1P3	1 dead channel	case(e)
M1N5	2 dead channels	case(e)
M1N1	2 preamplifiers not operating	case(d)
Silicon Strip Detector (tested with probe-station)		
p-side	4 pinholes : strips 2, 159, 162, 720	
n-side	1 pinhole : strip 451	

Figure 9: Identification and test results of module 1 components before the final assembly.

After the connection between all the components and the assembly have been made, the detection module is tested according to the method we have described and new mis-operating channels are determined. Results of this analysis are summarized in Tab.1 for module 1.

Detection module test results (module 1)		
p-side	11 strips are not connected to the readout electronic, 5 preamplifiers on ALICE chips are broken.	case(c) case(d)
n-side	1 chip M1N2 does not operate, 6 strips are not connected to the readout electronic, 4 preamplifiers on ALICE chips are broken.	case(f) case(c) case(d)

Table 1: Test results of module 1 analysis.

4.2 Analysis results

These defects are represented on Fig.4.2. We define the TAB connection number (abscissa of the graph) as the index of a copper strip, numbered from 1 to 128, of a single TAB tape. For the modules 2, 3 and 4 , hybrids are folded over the silicon strip detector. For modules 2 and 3, no analysis has been performed for the n-side due to readout problems. The analog output is disturbed and makes the analysis inefficient at determining the different types of defects.

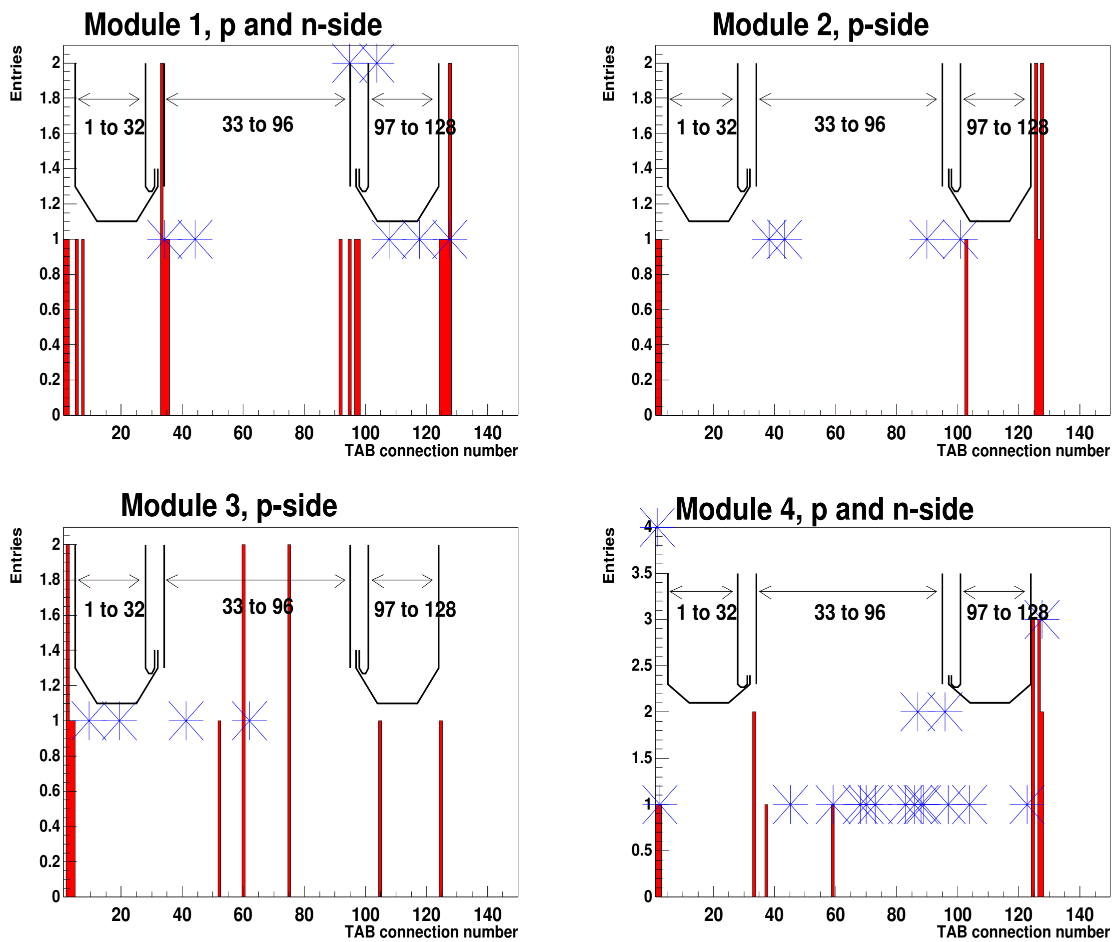

Figure 10: Not-connected strips (bars histogram) and mis-operating preamplifier (stars) versus the TAB connection index. The three schemes in the top of each picture, represent the three different types of copper strips geometry, straight or U-shaped, on TAB tape (cf. figure 1).

We clearly see that not-connected strips are almost systematically localized around the same areas with respect to TAB index. We suspect in this case several critical zones where connection seems to be more difficult to achieve, corresponding to TAB indexes (1,2,3 ...), (128,127,126, ...) and around 32 and 97. These areas correspond to connections on the edges of the TAB tape and/or on the edges of the readout chip.
Concerning the mis-operating preamplifiers, this defect spreads over the whole set of connections contrary to the localized not-connected strips. As we know that the analog inputs of the ALICE128C chip are not protected, we deduce that the preamplification transistor might be

destroyed by electrostatic discharges (ESD). The distribution of this defect could be explained with the random occurrence of an ESD. Results of this analysis are summarize in table 3 in terms of connection efficiency.

4.3 Test results of TABed ALICE128C chips

In table 2, we detail the tests performed at different steps of the assembly process on a set of ALICE128C chips. These chips have been used for the readout of module 4.

Probe tests performed by the manufacturer (AMS) and by IReS following delivery show that all the chips work correctly before any connection process. Then chips have been TABed to the tape and tested in their frame (see Fig.2). We can see that only 3 channels over 1536 have been destroyed in this process. Finally, module 4 has been tested with the same protocol as the one used for TABed chips. It demonstrates that most of the mis-operating channels come about during final assembly. Of course, mis-operating channels found with this method are in accordance with the result of test described in section 3. If the assumption that ESD induces mis-operating preamplifier is correct, these results show that ESD occurs during the connection of TABed chips with the detector.

Chip A128C identity	Probe tests AMS	Probe tests IReS	Chip on TAB tape dead channels (index)	Module 4 new dead channels (index)
M4P1	OK	OK	OK	128 : broken chip
M4P2	OK	OK	OK	1 (54)
M4P3	OK	OK	OK	2 (15,18)
M4P4	OK	OK	OK	3 (2,45,88)
M4P5	OK	OK	OK	OK
M4P6	OK	OK	OK	3 (53,63,84)
M4N6	OK	OK	1 (63)	1 (67)
M4N5	OK	OK	OK	2 (2,63)
M4N4	OK	OK	OK	3 (20,58,63)
M4N3	OK	OK	1 (20)	5 (1,15,16,22,48)
M4N2	OK	OK	1 (2)	2 (65,67)
M4N1	OK	OK	OK	2 (65,104)

Table 2: Summary of measurements on A128C chips during the assembly process.

5 Summary of the analysis results

The results of this analysis show (section 3, case (c)) that not-connected strips (NCstrips) have a systematic effect on left and right neighbouring strips. On Fig.7b, the strip 481 is not-connected to the readout electronic, noise increases for strips 480 and 482 : generally, $V(r_k)$ is 20% higher than mean noise in the area of the NCstrip. These effect is certainly due to the silicon strip detector and has no clear explanation for the moment.

When the preamplifier is broken (section 3, case (d)), charges flow directly into the power supplies lines of the preamplifier. The suspected ESD, responsible for these defects, may simply create a short-circuit between the preamplifier input and the power supplies.

The last point remaining to be discussed is the asymmetric behaviour of pinholes depending on which side they are located on. In case of pinhole, the coupling capacitor (e.g a silicon oxide layer between implanted and readout strips) is broken, thus a direct current is injected into the preamplifier of the readout chip and the sign of the DC component differs for each side :

$$\begin{array}{ll} \text{sign of } (i_{DC}^{in}) < 0 & \text{on n-side} \\ \text{sign of } (i_{DC}^{in}) > 0 & \text{on p-side} \end{array}$$

It has been tested in the lab using the facilities provided by the test frame of TABed chip (i.e a simple access to all the analog inputs). So we are able to inject a tunable DC current, positive or negative, in the preamplifier. At the same time, the channel was excited with A128C internal pulse generator. We observe the following behaviour : for a positive current, the preamplifier operates up to $\sim$ 350 nA, but the analog output signal is modified and the channel gain is lower. For a negative current, the preamplifier is instantaneously blocked when a current of few nA is injected. No increasing noise effects occurs on neighbouring channels as it can be seen when the chip is connected to a silicon strip detector.
For a detection-module, not-connected strips and pinholes on n-side lead to the same noise enhancement on neighbouring strips.

The results of the analysis of defects is summarized in the following table. For these first four TABed modules, a good connection efficiency is obtained : mean value is 98% (excluding the problem of dead chip). Especially if we consider that some bonding parameters have been tuned during this step of prototype assembly.

	Module 1		Module 2		Module 3		Module 4	
detector-side	P	N	P	N	P	N	P	N
Not-connected strips	11	6	8	(<5)	11	(-)	5	9
Dead preamplifier	5	4	4	(<5)	4	(-)	9	15
Dead chip	0	1	0	1	0	0	1	0
Efficiency	97.9 %	82.1 %	98.7 %	> 82 %	98.1 %	(-)	81.5 %	96.9 %

Table 3: Quantitative summary of measured defects on 4 detection modules and corresponding connection efficiency.

6 Conclusions

For the time being, only a few modules using TAB connection technique have been assembled (a total of 6), and most of them immediatly operated well. Nevertheless it is possible to get formal conclusions about the specific points where weaknesses of TAB process are clearly identified. The first point concerns the mis-operating preamplifiers, these defects appear mainly during the connections of TABed chips to the detector. They are certainly due to ESD in the analog input of the readout chip. This assumption seems to be confirmed by this analysis. The second point deals with not-connected strips, those defects are well localized on the TAB tape,

tending to prove that connections are more difficult to achieve in edges zones. Improvement of the process will certainly solve this problem. The results showned in table 3 exhibits also the problem of broken chips after mounting. This is due to bad connections between chips and hybrid : if a connection used for control signal or for power supplies is defective, the chip will not operate. This is critical in the way that the information on 128 strips is lost. Anyway these connections (readout chip to hybrids) are simpler to perform, and will easily be solved with process improvement. The last produced modules (5 and 6) do not exhibit this problem anymore.
The crosstalk between strips has also been tested, results related in [7] demonstrate that no significant impact of TAB on correlated noise has been observed.

In order to have a full module characterization in a simpler way as the one described in section 3, a test bench equipped with a control-motion laser-source has been built. The TAB defect examination is performed with the help of noise runs and based on the analysis described in this paper. Automatic examination will be easily done with the laser source (instead of β-source) and the internal test pulse generator of the ALICE128C chip.

References

[1] R. Bellwied et al. (the SDDA collaboration),
The performance of the SVT-SDDs in AGS Experiment 896
STAR note SN0321.

[2] S. Pandey and the STAR collaboration.,
The STAR Silicon Drift Vertex Detector
Nuclear Physics **A661** (1999), 686c-689c.

[3] A. Boucham et al.,
Proposal for a Silicon Strip Detector for STAR
STAR note SN0400.

[4] C. Roy, L. Martin, W. Pinganaud,
Onset of Neutral Strange Particle Reconstruction Including the SSD
STAR note SN0421.

[5] L. Hebrard and al.,
ALICE 128C : A CMOS Full Custom for the Readout of the Silicon Strip Detector in the Alice Experiment
Proceedings of the 3rd Workshop on Electronics for LHC Experiments, Imperial College, London, September 1997 CERN/LHCC/97-60,p.173.

[6] S. Bouvier,
TAB : a packaging technology used for silicon strip detector to front end electronics interconnection
Proceedings of the 4^{th} workshop on electronics for LHC experiments, Rome, September 21-25, 1998.

[7] W. Pinganaud,
Contribution au développement du détecteur au silicium micropistes de l'expérience STAR au RHIC
Université de Nantes, Faculté des Sciences et Techniques, Phd Thesis, October 2000.
available at http:star.in2p3.frSTAR_documents.html

[8] D. Bonnet and al.,
Control system of silicon microstrip layer for the STAR experiment
Proceedings of ICALEPS'99, Trieste, October 1999.

[9] C. Suire and al.,
Off- and in-beam tests of Silicon-strip Detectors for the ALICE experiment at LHC
ALICE/99-22 Internal NOTE/ITS, May 1999.

[10] ALICE collaboration,
ALICE Technical Design Report of the Time Projection Chamber
CERN/LHCC 2000-001 ALICE TDR 7.